Title

Topological quantum properties of chiral crystals

Journal

Nature Materials, 17(11)

ISSN

1476-1122

Authors

Chang, Guoqing

Wieder, Benjamin J

Schindler, Frank

et al.

Publication Date

2018-11-01

DOI

10.1038/s41563-018-0169-3

Peer reviewed

Topological quantum properties of chiral crystals

Guoqing Chang[1,2,3,4,12], Benjamin J. Wieder[5,6,7,12], Frank Schindler[8,12], Daniel S. Sanchez[1], Ilya Belopolski[1], Shin-Ming Huang[9], Bahadur Singh[2,3], Di Wu[2,3], Tay-Rong Chang[10], Titus Neupert[8], Su-Yang Xu[1]*, Hsin Lin[2,3,4]* and M. Zahid Hasan[1,11]*

Chiral crystals are materials with a lattice structure that has a well-defined handedness due to the lack of inversion, mirror or other roto-inversion symmetries. Although it has been shown that the presence of crystalline symmetries can protect topo- logical band crossings, the topological electronic properties of chiral crystals remain largely uncharacterized. Here we show that Kramers–Weyl fermions are a universal topological electronic property of all non-magnetic chiral crystals with spin–orbit coupling and are guaranteed by structural chirality, lattice translation and time-reversal symmetry. Unlike conventional Weyl fermions, they appear at time-reversal-invariant momenta. We identify representative chiral materials in 33 of the 65 chiral space groups in which Kramers–Weyl fermions are relevant to the low-energy physics. We determine that all point-like nodal degeneracies in non-magnetic chiral crystals with relevant spin–orbit coupling carry non-trivial Chern numbers. Kramers–Weyl materials can exhibit a monopole-like electron spin texture and topologically non-trivial bulk Fermi surfaces over an unusually large energy window.

The spatial structures of three-dimensional crystal lattices are characterized by a finite set of possible symmetries that give rise to the 230 space groups (SGs) for non-magnetic materials[1,2]. In this work, we examine the properties of the SGs that char- acterize crystal structures with a sense of handedness, or structural chirality (Fig. 1a). Spatial inversion, mirror reflection and roto-inversion, that is, a combination of inversion and rotation, all invert structural chirality in crystals[3]. Of these 230 groups, 65 SGs are free of chirality-inverting symmetries. These chiral SGs correspondingly characterize structurally chiral lattices (Supplementary Section A).

The electronic properties of chiral crystals have been previously recognized as supporting a wide range of phenomena: chi- ral magnets support skyrmions[4], chiral metals show non-local and non-reciprocal electron transport[5,6] and chiral crystals also exhibit optical activity and magnetochiral dichroism[7]. These unusual prop- erties mean it is of great interest to search for possible topological electronic properties in chiral crystals. In this work, we show that structural chirality leads to a universal topological electronic property of all non-magnetic chiral crystals with spin–orbit coupling (SOC), namely, Kramers–Weyl fermions. Although most of the recent theoretical advances in topological semimetals have related band structures to the presence of additional crystalline symmetries (for example, rotation, reflection, non-symmorphic momenta (TRIMs) are Kramers–Weyl nodes with a quantized chi- ral charge $|C| = 1$. We then use group theory, briefly in this section and exhaustively in Supplementary Section B, to generalize this result and demonstrate that the same arguments apply to all of the TRIMs in symmorphic chiral SGs.

SG 16 characterizes a non-centrosymmetric orthorhombic crys- tal structure with two-fold rotation symmetries along each principle axis, x, y and z. Considering all the symmetry-allowed nearest- neighbour hopping terms, the tight-binding Hamiltonian reads:

$$H(\mathbf{k}) = \sum_{i=x,y,z} t_i^1 \cos(k_i) + t_i^s \sin(k_i)\,\sigma_i \qquad (1)$$

with $t_i^1 \neq t_j^1 \neq t_{i_s}^s \neq t_j^s \neq t_i^s \; \forall\, i \neq j$. Here t_i^1 denotes the s-orbital-like hopping strength and t_i^s is a spin–orbit term. By examining the bands at each TRIM at the $\mathbf{k}\cdot\mathbf{p}$ level, we observe that each TRIM hosts a Weyl node described by:

$$H_{\mathbf{k}\cdot\mathbf{p}} = \sum_{i=x,y,z} \left[u_i \left(1 - \frac{k^2}{2}\right) + v_i k_i \sigma_i \right] \qquad (2)$$

symmetries)[8–24], we highlight a class of nodal fermions

enforced by structural chiral- ity, and therefore by the absence of particular crystal symmetries.

Tight-binding model of a SOC coupled chiral crystal Without loss of generality, we present a tight-binding model in the symmorphicchiral SG 16 (*P*222) asarepresentativeexample. Weshow that in SG 16, all Kramers degeneracies at time-reversal-invariant

where each TRIM has the same magnitude of u_i and v_i inherited from the lattice hopping parameters, but different TRIM-specific signs. In Fig. 1c,d, we show the band structure for this tight-bind- ing model in the absence and presence of SOC, respectively. The inclusion of SOC splits the spin-degenerate band in Fig. 1c and generates isolated two-fold-degenerate Kramers–Weyl nodes at all of the TRIMs (Fig. 1d)[18]. To determine the chiral charge of each Kramers–Weyl node, we examine the direction of the wrapping of

[1]Laboratory for Topological Quantum Matter and Advanced Spectroscopy (B7), Department of Physics, Princeton University, Princeton, NJ, USA. [2]Centre for Advanced 2D Materials and Graphene Research Centre, National University of Singapore, Singapore, Singapore. [3]Department of Physics, National University of Singapore, Singapore, Singapore. [4]Institute of Physics, Academia Sinica, Taipei, Taiwan. [5]Department of Physics, Princeton University, Princeton, NJ, USA. [6]Nordita, Center for Quantum Materials, KTH Royal Institute of Technology and Stockholm University, Stockholm,
Sweden. [7]Department of Physics and Astronomy, University of Pennsylvania, Philadelphia, PA, USA. [8]Department of Physics, University of Zurich, Zurich, Switzerland. [9]Department of Physics, National Sun Yat-Sen University, Kaohsiung, Taiwan. [10]Department of Physics, National Cheng Kung University, Tainan, Taiwan. [11]Lawrence Berkeley National Laboratory, Berkeley, CA, USA. [12]These authors contributed equally: Guoqing Chang, Benjamin J. Wieder, Frank Schindler.
*e-mail: xusuyang1962@gmail.com; nilnish@gmail.com; mzhasan@princeton.edu

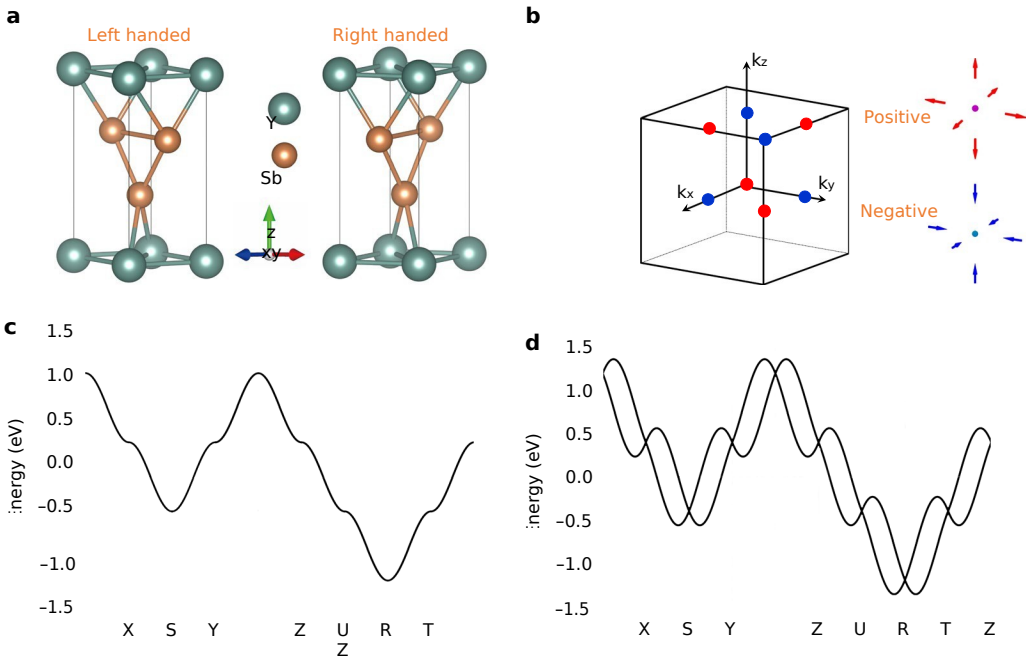

Fig. 1 | Structural chirality, topological chirality and Kramers–Weyl fermions. **a**, Structurally chiral crystals have a distinct handedness, and are therefore characterized by an absence of inversion, mirror or other roto-inversion symmetries[3]. **b**, Topologically chiral fermions act as monopoles or antimonopoles of Berry curvature. They are characterized by a quantized chiral charge, that is, the quantized Chern number of the occupied bands on a closed surface in momentum space that surrounds the chiral fermion. We found all non-magnetic chiral crystals with SOC host topological chiral fermions at their TRIMs. **c**, The band structure for the SG 16 tight-binding model in the absence of SOC is characterized by a single band with a two-fold spin degeneracy. **d**, The inclusion of SOC splits the bands of this structurally chiral model everywhere except at the TRIMs, where Kramers theorem mandates that the bands remain doubly degenerate. We found that these nodal degeneracies carry the same quantized chiral charge as conventional Weyl fermions, and therefore designate them Kramers–Weyl fermions.

Berry curvature given by the relative signs of the $\{v_i\}$ (the overall sign exchanges the Bloch states of the upper and lower bands) to find the Chern number:

$$C = \left| \prod_{i=x,y,z} \mathrm{sgn}\,(v_i) \right| \quad (3)$$

This result indicates the chiral charge $C = +1 \times \mathrm{sgn}\,(t^s_x t^s_y t^s_z)$ for the Kramers pairs at TRIM points Γ, S, U and T, and $C = -1 \times \mathrm{sgn}\,(t^s_x t^s_y t^s_z)$ for the pairs at X, Y, Z and R, as illustrated in Fig. 1b. The sign of C at Γ reflects the signs of the $\{t_i\}$ for the position–space lattice. Thus, the chirality of the atomic positions is directly responsible for defining the handedness of the Kramers–Weyl node at Γ and therefore, by the pattern of alternating signs, at all of the other TRIMs as well.

As our determination of $C = \pm 1$ only relied on the two-fold degeneracy and linear dispersion of equation (2), we deduce that any such degeneracy must be a Weyl node. More precisely, as the little groups of all eight TRIMs in SG 16 are isomorphic to the same chiral point group 222, which with spinful T-symmetry only has a single two-dimensional co-representation[2,22], we conclude that any TRIM with a little group isomorphic to point group 222 must also host Kramer–Weyl fermions. Tuning parameters such that $u_i = 0$ and $v_i = v_j$ for all i and j, this $\mathbf{k}\cdot\mathbf{p}$ theory becomes isotropic, and thus invariant under the action of any chiral point group. Taken together, this implies that the little group of the Γ point in an arbitrary chiral crystal, which is

that describe Kramers–Weyl fermions[2,19,20,23]. We also show in Supplementary Sections C and D that Kramers–Weyl fermions with $|C| = 3$ and non-linear dispersion are permitted in chiral point groups with three- and six-fold rotation symmetries, and in Supplementary Section D we identify the irreducible co-represen- tations of these higher-Chern-number Kramers–Weyl fermions. Previous reports also exploited similar simple models in discussing Weyl fermions[25,26]. However, they did not explore the relations of the little groups at the TRIMs with each other, and more impor- tantly they did not recognize that their isomorphisms to chiral point groups allow the generalization to other crystal systems.

In non-symmorphic chiral crystals, these arguments become modified away from the Γ point, and the Kramers–Weyl nodes can become obscured by additional band degeneracies. Consider, for example, the chiral SG 19 ($P2_12_12_1$), which differs from SG 16 in that all of its two-fold rotations are, instead, non-symmorphic screws: $s_x = \{C_{2x}|\frac{1}{2}\,\frac{1}{2}\,0\}$, $s_y = \{C_{2y}|0\,\frac{1}{2}\,\frac{1}{2}\}$ and $s_z = \{C_{2z}|\frac{1}{2}\,0\,\frac{1}{2}\}$. In reciprocal space, $\frac{2\pi}{2}$ $\frac{2\pi}{2}$ $\frac{2\pi}{2}$ the little groups

isomorphic to the point group of that crystal, and every TRIM point in symmorphic chiral crystals, which host symmetry algebras unmodified by the projections of fractional lattice transla- tions, must always allow at least one irreducible co-representation of a Kramers–Weyl fermion. In Supplementary Section B, we explicitly confirm this conclusion and list the irreducible co-representations

$s_i \times T$ are valid symmetry operations that map a **k** point to itself on the $k_i = 0, \pi$ planes. When acting on a Bloch eigenstate of the Hamiltonian, $(s_i T)^2 = e^{-ik_i}$ enforces two-fold Kramers degeneracies throughout all three $k_i = \pi$ planes. TRIMs that belong to exactly two nodal planes will host four-fold degeneracies, due to the algebra of the screw rotations at those **k** points. In Supplementary Sections E and F, we examine these nodal surfaces in detail and determine that they exhibit non-zero chiral charges[27].

We also note that in certain achiral SGs, it is possible for some of the TRIMs to still have little groups isomorphic to chiral point groups due to the relationship between the SG roto-inversion axes, mirror planes, and the reciprocal lattice vectors. In Supplementary Section G, we explore this possibility and present examples of Kramers–Weyl fermions in achiral crystals.

Table 1 | Representative topological chiral crystals with Kramers–Weyl fermions in symmorphic chiral SGs

SG	Material (code)	Number of collections in the ICSD	SG	Material (code)	Number of collections in the ICSD
	$Li_6CuB_4O_{10}$ (249215)	492	146	β-Ag_3IS (93431)	307
3	Pb_3GeO_5 (200517)	58	149	$RbGeIO_6$ (73613)	40
5	$Ca_2B_5Os_3$ (59229)	539	150	Tl_2TeO_6 (4321)	314
16	$AlPS_4$ (15910)	13	155	Ag_3BO_3 (26521)	244
21	YSb_2 (651733)	51	168	$K_2Ta_4F_4O_9$ (8204)	3
22	$ThOs_2B_2$ (601346)	55	177	$PbS_2O{\cdot}4H_2O$ (68630)	3
23	$BaAg_2SnSe_4$ (170856)	28	195	SnI_4 (18010)	29
75	$K_4CuV_5ClO_{15}$ (401042)	27	196	α-Cu_2Se (59955)	47
79	$AgBi(Cr_2O_7)_2$ (14233)	45	197	m-Bi_2O_3 (27152)	174
89	–	3	207	$RbNO_3$ (60966)	1
97	Ta_2Se_8I (35190)	9	209	Na_3PO_4 (14090)	8
143	RbW_3O_9 (96421)	112	211	$NiHg_4$ (151197)	3

We list all 24 symmorphic chiral SGs and, where possible, material candidates from the ICSD[30]. All the compounds listed in the table host Kramers–Weyl fermions. Among them, the compounds in italic are (semi)metals or small-gap insulators with clean Fermi surfaces and Kramers–Weyl fermions near the Fermi level; their electronic structures are shown in Supplementary Section J. The numbers in brackets are the ICSD collection codes. The SGs in bold may also host additional unconventional four-fold-degenerate chiral fermions at TRIMs with little groups isomorphic to chiral point groups[19,23,24]. SGs 195, 196 and 197 have TRIM-point little groups isomorphic to chiral point group 23 (*T*)[23,24]. SGs 207, 209 and 211 have TRIM-point little groups isomorphic to chiral point group 432 (*O*)[19].

Apart from conventional $|C| = 1$ Weyl fermions, all the degener- acies in non-magnetic crystals are captured by the set of irreducible (co)representations[22]. For each of these degeneracies, a separate cal- culation of the chiral charge can then be performed. Remarkably, by exhaustively enumerating all of the irreducible (co)representations of the 65 chiral SGs and comparing them to the set of known chiral fermions, now including the Kramers–Weyl fermions highlighted in this work, we find that all the point degeneracies in chiral SGs exhibit a non-zero chiral charge (Supplementary Section N). Specifically, they are either conventional $|C| = 1$ Weyl fermions[11–13], double- or triple-Weyl fermions on rotation axes[16], unconventional chiral fer- mions at high-symmetry crystal momenta[19,23,24] or Kramers–Weyl fermions. In Supplementary Section O, we compare the symmetry and topology of the Kramers–Weyl fermions with previous exam- ples of conventional and unconventional chiral fermions.

Intrinsic-filling Kramers–Weyl metals also represent the sim- plest examples of filling-enforced semimetals[18]. Although previ- ous works focused on the role of non-symmorphic symmetries in generating large and exotic band connectivities[18,19,22,23], we found in this work that even the simplest filling restriction—that is, a *T*-symmetric crystal with an odd number of electrons per unit cell—must be gapless and can be used to predict materials with Weyl fermions. A deeper theoretical understanding of this preference may provide greater insight into the appearance of Mott insulating and other interacting phases in certain filling- enforced semimetals[28,29].

Kramers–Weyl physics in known chiral materials

Consulting the Inorganic Crystal Structure Database (ICSD)[30], we identify in Tables 1 and 2 representative examples of previously synthesized chiral crystals and highlight in italic the materials in which Kramers–Weyl fermions are relevant to the low-energy phys- ics, which we demonstrate with calculated electronic structures pro- vided in Supplementary Section J. The number of materials varies greatly across the 65 chiral SGs. We found that a large number of known chiral crystals have SGs 4, 19, 173 and 198, whereas SGs 89, 93, 153, 171 and 172 are devoid of promising material candidates.

Among the chiral materials listed in Tables 1 and 2, there are both chiral metals and insulators. Although the Kramers–Weyl nodes in insulators are not generically relevant to transport experiments,

they may still be probed with angle-resolved photoemission spec- troscopy[8,31-33], scanning tunnelling microscopy[9], resonant inelastic X-ray scattering[34], neutron scattering[35] or by optical measurements[36]. Furthermore, when the Kramers–Weyl nodes of an insulator are near the Fermi level, they could also be studied in transport experi- ments[37] after slight electron or hole doping.

We present two material candidates particularly representative of this physics: a chiral metal and a chiral insulator with spectro- scopically accessible Kramers–Weyl Fermi arcs. The band struc- ture of the symmorphic compound Ag_3BO_3 (no. 26521) (SG 155) is plotted in Fig. 2b,c without and with SOC, respectively; we highlight the Kramers–Weyl nodes with orange circles. As in con- ventional Weyl semimetals, Kramers–Weyl points also give rise to Fermi arcs which, on surfaces for which bulk TRIMs project onto the surface TRIM points, must necessarily appear in time-reversed pairs. We identified the insulating compound $AgBi(Cr_2O_7)_2$ (no. 14233) in SG 79 as representative of this physics. The bulk elec- tronic structure of $AgBi(Cr_2O_7)_2$ in the absence and presence of SOC is shown in Fig. 2f,g, respectively. We confirmed the existence of time-reversed pairs of Fermi arcs at about −0.23 eV below the Fermi energy on the (110) surface (Fig. 2i). A loop taken around one of the surface TRIMs exhibits a projected Chern number of $C = +2$, which necessitates the existence of two Fermi arcs (Fig. 2j). We note that, because the Kramers–Weyl nodes are pinned to the TRIMs, chiral crystals can, in principle, support the longest pos- sible Fermi arcs, and therefore span the entire surface Brillouin zone like those in the unconventional chiral semimetal β-RhSi (refs [23,24]). However, this is very challenging to realize in real mate- rials, for which the bandwidths, determined by the hopping ampli- tudes, are typically much greater than the spin splitting, which is determined by the strength of the SOC (Supplementary Section I).

Quantum phenomena in chiral crystals

Here we describe five phenomena relevant to the Kramers–Weyl fermions in chiral crystals. Phenomena 1 and 2 are unique to Kramers–Weyl fermions and have not been proposed previously. Phenomena 3–5 were proposed in previous works and are not unique to Kramers–Weyl fermions. Instead, we highlight how Kramers–Weyl fermions provide a previously unrecognized plat- form for realizing these phenomena.

Table 2 | Representative topological chiral crystals with Kramers–Weyl fermions in non-symmorphic chiral SGs

SG	Material (code)	Number of collections in the ICSD	SG	Material (code)	Number of collections in the ICSD
4	$BaCu_2Te_2O_6Cl_2$ (85786)	912	152	$IrGe_4$ (53655)	408
17	$Ba_2Cu_3YPb_2O_8$ (66088)	29	153	–	1
18	Pd_7Se_4 (77897)	177	154	$SrIr_2P_2$ (73531)	159
19	α-Ag_2Se (261822)	1145	169	α-In_2Se_3 (82203)	55
20	$CsCuBr_3$ (10184)	219	170	$BaN_2O_4{\cdot}H_2O$ (201484)	14
24	K_2PdSe_{10} (71947)	10	171	–	4
76	$TlBO_2$ (36404)	64	172	–	1
77	$MgB_2O(OH)_6$ (24920)	9	173	$CuLa_4S_7$ (628240)	1238
78	$Sr_2As_2O_7$ (190008)	22	178	Hf_5Ir_3 (638575)	55
80	β-NbO_2 (35181)	22	179	$Na_3B_4O_7Br$ (252106)	32
90	$Na_4Ti_2Si_8O_{22}{\cdot}4H_2O$ (240912)	20	180	$NbGe_2$ (16503)	241
91	Ag_3SbO_4 (417675)	31	181	WAl_2 (173662)	48
92	$MgAs_4$ (1079)	309	182	$PbRbIO_6$ (73615)	217
93	–	-	198	β-RhSi (79233)	766
94	$H_6NaB_6{\cdot}2H_2O$ (39376)	7	199	$K_2Sn_2O_3$ (40463)	104
95	$H_4Ca_2AsF_{13}$ (415156)	15	208	Zn_3As_2 (24486)	9
96	m-Cu_2S (16550)	105	210	H_6TeO_6 (16435)	7
98	$CdAs_2$ (16037)	25	212	Li_2Pd_3B (84931)	152
144	$LaBSiO_5$ (39756)	89	213	Mg_3Ru_2 (260022)	221
145	BiB_2O_4F (172481)	32	214	Ag_3Se_2Au (171959)	33
151	$DyAl_3Cl_{12}$ (65975)	48			

We list all 41 non-symmorphic chiral SGs and, where possible, material candidates from the ICSD[30]. The details are given in Table 1. SGs 198 and 199 have TRIM-point little groups isomorphic to chiral point group 23 (*T*)[23,24]. SGs 208, 210, 212, 213 and 214 have TRIM-point little groups isomorphic to chiral point group 432 (*O*)[19].

Spin texture of Kramers–Weyl fermions. The most gen- eral Hamiltonian of a |C| = 1 Weyl fermion can be written as $H_{\text{Weyl}}(\mathbf{k}) = v_i k_i \sigma_0 + A_{ij} k_i \sigma_j$, where A_{ij} and v_i are real numbers and sums over repeated indices $i,j = x,y,z$ are implied. For the Weyl nodes in a band-inversion Weyl semimetal, σ represents only an effective pseudo-spin degree of freedom, which is very difficult to measure in a momentum-resolved fashion. The physical spin, which can be directly measured by spin-resolved angle-resolved photoemission spectroscopy, is distinct from this pseudo-spin.

Conversely, in the $\mathbf{k}\cdot\mathbf{p}$ theory of Kramers–Weyl fermions, σ represents the true electron spin in the limit in which the energy scale of SOC is much smaller than the interband separation in the absence of SOC (Supplementary Section L). Remarkably, we found that, in this limit, the chiral charge of a Kramers–Weyl fermion can be directly probed by measuring the spin texture. This is a unique property of Kramers–Weyl fermions. Specifically, the physical spin on Fermi surfaces that enclose a Kramers–Weyl node sweeps out the full unit sphere. As the chiral charge is given by $C = \text{sgn}[\det(A)]$, C can be directly obtained by measuring the spin polarization $\mathbf{S}_\mathbf{k} = (\mathbf{k}|\sigma|\mathbf{k})$ near the Kramers–Weyl nodes by calculating:

$$C^{\text{Kramers-Weyl}} = -\text{sign}(k)\,\text{sign}\,(\mathbf{S}_{(k,0,0)} \times \mathbf{S}_{(0,k,0)} \cdot \mathbf{S}_{(0,0,k)}) \quad (4)$$

points inward along all three principal directions, or it points inward along one direction and outward along the other two direc- tions. In addition, T-symmetry enforces $v_i = 0$ for Kramers–Weyl fermions, and thus the Kramers–Weyl cone cannot be 'tilted' in momentum space[38].

Using first-principles calculations, we confirmed the presence of this spin texture in the Kramers–Weyl fermions in Ag_2Se, and con- trast it here with that of the conventional band-inversion induced Weyl fermions in TaAs (Fig. 3e,f). In Supplementary Section M, we further show that the real spin–momentum locking of Kramers– Weyl nodes can lead to a large spin Hall conductivity.

Unusually large topologically non-trivial energy windows. A Fermi pocket that encloses a single Weyl node carries a quantized Chern number. Recent reports[39–41] highlighted that such Fermi pockets can lead to unique transport and symmetry-breaking phe- nomena, which include magnetic breakdowns[39], unconventional quantum oscillations[40], chiral charge-density waves[41] and giant spin Hall effects[42].

For a conventional band-inversion-induced Weyl semimetal, isolated chiral Fermi surfaces may only be realized at energies close to the Weyl nodes, which typically are only separated by a few hun-

Moreover, in the presence of additional rotational symme- tries, Kramers-Weyl fermions exhibit spin–momentum locking (Supplementary Section L gives a detailed discussion). Specifically, for a $C = +1$ Kramers–Weyl node, the spin either points outward along all three principal directions (for example, k_x, k_y and k_z) or it points outward along one direction and inward along the other two directions; for a $C = -1$ Kramers–Weyl node, the spin either

dredths of the Brillouin zone in momentum, and at less than the order of 100 meV in energy[31,32]. Therefore, it is quite challenging to realize band-inversion Weyl semimetals with isolated chiral Fermi surfaces; only TaAs and TaP display well-isolated chiral surfaces, whereas in other materials, such as NbP, NbAs and WTe_2, the chem- ical potential misses the narrow energy window defined by the weak band inversion[31,32,38].

In stark contrast, in chiral crystals, isolated Fermi surfaces with a non-vanishing Chern number can form at any energy between

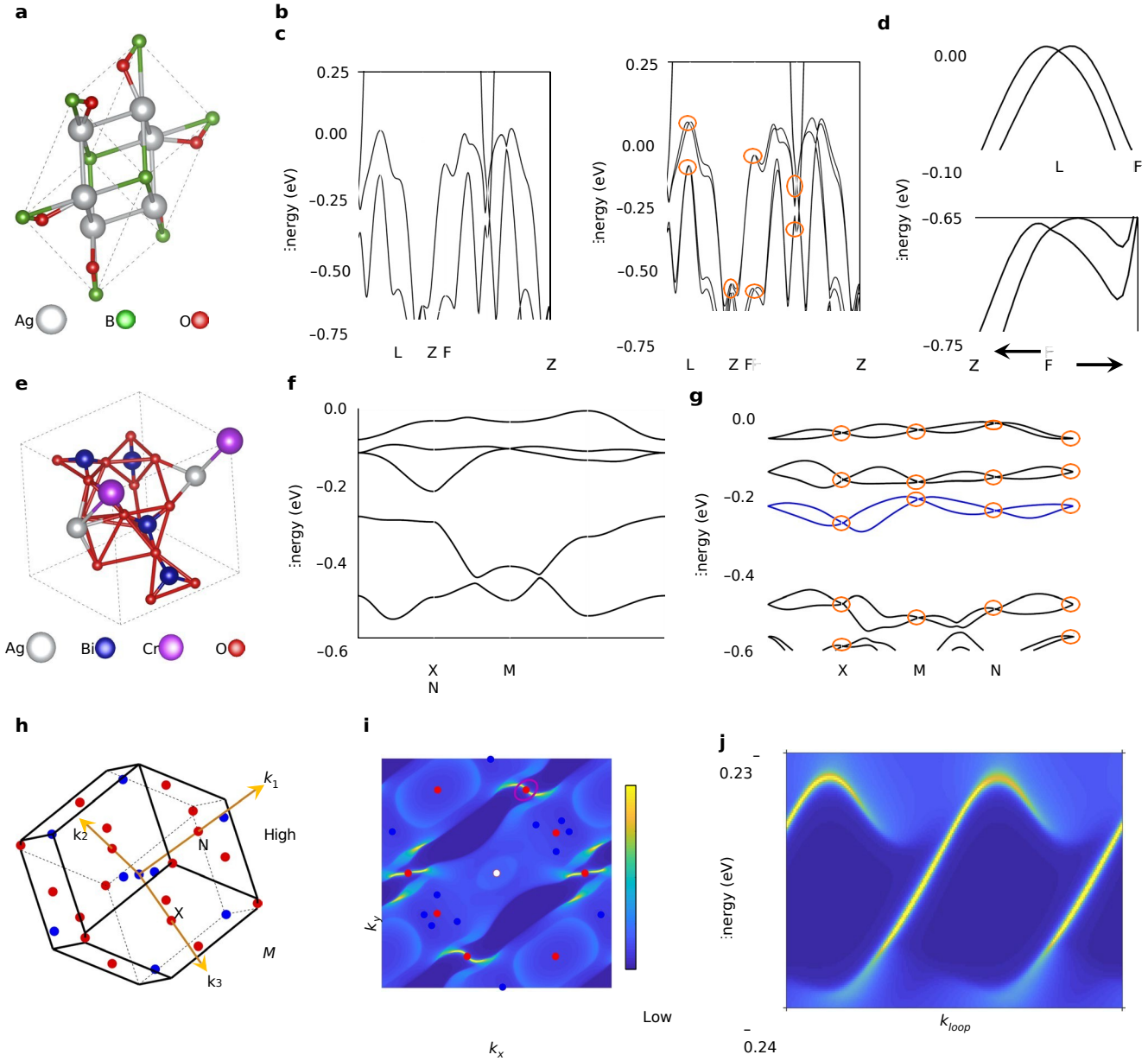

Fig. 2 | Band topology and Fermi arcs of Kramers–Weyl material candidates. **a**, The chiral crystal Ag_3BO_3 in SG 155. **b**,**c**, The band structures of Ag_3BO_3 passing through TRIMs in the absence (**b**) and presence (**c**) of SOC, respectively. All of the TRIMs in Ag_3BO_3 host isolated Kramers–Weyl nodes in the presence of SOC, as indicated by the orange circles. **d**, The Kramers–Weyl band structures in the vicinity of L (top) and F (bottom). **e**–**g**, The crystal (**e**), electronic structures of $AgBi(Cr_2O_7)_2$ in SG 79 in the absence (**f**) and presence (**g**) of SOC. **h**, Momentum-space distribution and chiralities of the Weyl nodes in $AgBi(Cr_2O_7)_2$ between the two blue bands in **g**. The red and blue circles indicate Weyl nodes of opposite chiral charges. **i**, The (110) surface state spectral function of $AgBi(Cr_2O_7)_2$ at $E = -0.235$ eV. The Fermi arc surface states that connect the projections of the two distinct bulk pockets are clearly visible. The projected charges of red (blue) circles are +2 (−1). **j**, The surface spectral function along the k path highlighted in **i** exhibits a +2 winding number, consistent with the pair of chiral Fermi arcs observed in **i**.

the highest and the lowest Kramers–Weyl nodes or unconventional chiral fermions in a set of connected bands. The scale of this energy window is governed by the lattice hopping, typically much larger than the accessible scale of band inversion in conventional Weyl semimetals, and the splitting between Fermi surfaces of opposite Chern number is, instead, determined by the strength of the SOC (Fig. 1d and Supplementary Sections H and I).

Quantized circular photogalvanic current. In a recent theoretical work, a quantized circular photogalvanic response effect (CPGE) in roto-inversion-free Weyl semimetals was proposed[36], in which Weyl nodes of one chirality sit at the Fermi level and nodes of the oppo- site chirality lie energetically far away from it. A crucial limitation that has hindered the realization of this phenomena is the lack of viable materials. Indeed, very few Weyl semimetals are known to

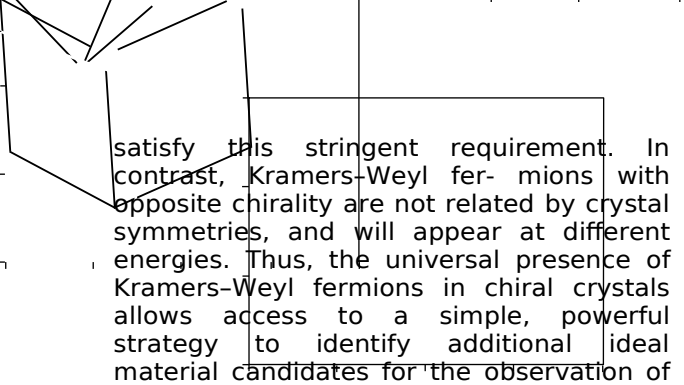

satisfy this stringent requirement. In contrast, Kramers–Weyl fer- mions with opposite chirality are not related by crystal symmetries, and will appear at different energies. Thus, the universal presence of Kramers–Weyl fermions in chiral crystals allows access to a simple, powerful strategy to identify additional ideal material candidates for the observation of quantized photocurrent: identify semimetal- lic chiral crystals in which a Kramers–Weyl node is isolated at the intrinsic chemical potential, or identify narrow-gap semiconduct- ing chiral crystals in which a Kramers–Weyl node can be isolated by moderate electron or hole doping.

We present α-$Ag_2Se_{0.3}Te_{0.7}$ (SG 19) as an example for doping- enabled photocurrent (Fig. 3). As discussed in Supplementary Section F, crystals in SG 19 display chiral Kramers–Weyl nodes at Γ, and two-fold-degenerate chiral nodal planes along the Brillouin zone boundaries ($k_i = \pi$) (Fig. 3a,b). With slight electron doping,

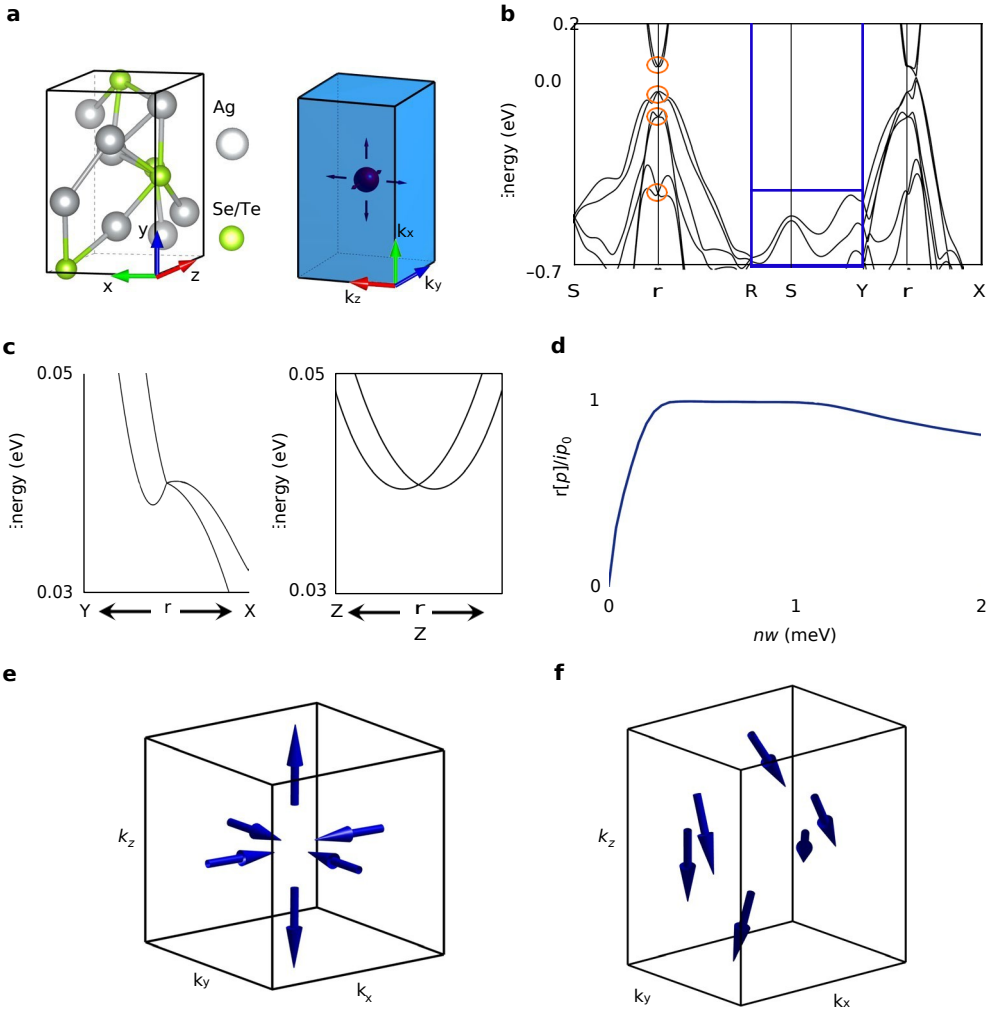

Fig. 3 | Quantized circular photogalvanic current and topological spin–momentum locking. **a**, The chiral crystal α-$Ag_2Se_{0.3}Te_{0.7}$ (left) and the chiral fermions in α-$Ag_2Se_{0.3}Te_{0.7}$ (right) where the Γ point allows an isolated Kramers–Weyl node and the Brillouin zone boundaries feature a nodal surface with a non-zero chiral charge (Supplementary Sections E and F). **b**, The band structure of α-$Ag_2Se_{0.3}Te_{0.7}$ with SOC. The Kramers–Weyl fermions at Γ are highlighted by orange circles. The chiral nodal surfaces are indicated by the blue box. **c**, Bands in the vicinity of the Γ point. **d**, Quantized circular photogalvanic currents induced by the Kramers–Weyl fermions in slightly electron-doped α-$Ag_2Se_{0.3-\delta}Te_{0.7}$ (δ = 0.16%) (whose Fermi level is at the energy of the Kramers–Weyl fermion of conduction bands). β is the multiband gyrotropic photocurrent tensor (Methods) and Tr[β] means the trace of the photocurrent tensor β. $\beta_0 = \pi e^3/h^2$ is a quantized constant, where e and h are the electron charge and the Planck constant. Tr[β]/$i\beta_0$ is dimensionless and should reach an integer if the photocurrent is quantized. **e**,**f**, Real spin along the three principle axes (k_x, k_y and k_z) for the Kramers–Weyl node near the Fermi level in α-Ag_2Se (**e**) and a conventional Weyl node in TaAs (**f**).

one can shift the Fermi level to the Kramers–Weyl fermions. The calculated photogalvanic current of α-$Ag_2Se_{0.3-\delta}Te_{0.7}$ (δ = 0.16%) (Fig. 3d) exhibits a quantized value in the terahertz photon ener- gies (~1 meV)[43]. Continuing with this strategy, we easily identify 16 additional chiral materials for the observation of Kramers–Weyl- enabled quantized photocurrent. These compounds are enumerated along with their band structures in Supplementary Section J.

The chiral magnetic effects. The chiral and gyrotropic effects are linear responses in Weyl semimetals to electromagnetic waves[44,45]. In these chiral magnetic effects, a dissipationless current arises in response to an alternating magnetic field. These effects are cru- cially reliant on the same energetic restrictions as the CPGE in the previous section: that Weyl nodes of different chiralities lie at dif- ferent energies. Like the CPGE, the realization of these effects has been hindered due to the absence of ideal material platforms. Our proposal of Kramers–Weyl fermions immediately provides a fea- sible platform in which to probe these response effects.

Other exotic phenomena in chiral crystals. Finally, we propose that Kramers–Weyl fermions may offer a way to systematically con- trol and modulate a number of symmetry-allowed phenomena in structurally chiral crystals, including the magnetochiral and mag- netoelectric effects[5,6]. Although these phenomena can still occur in a chiral crystal in the absence of a Weyl node near the Fermi energy, recent theoretical works highlight that the presence of a strong Berry curvature can dramatically enhance the magnitude of these effects[6]. In addition, the presence of Kramers–Weyl fermions near the Fermi energy may offer the possibility to study superconduct- ing pairing on Fermi surfaces with a non-zero Chern number[46,47], which may provide a promising recipe for engineering unconven- tional superconductivity[48].

Conclusion

In this work, we uncovered a fundamental consequence of the com- bination of *T* symmetry and structural chirality in crystals with a spin–orbit interaction. We found that in chiral crystals, the TRIM

points host Kramers–Weyl and other unconventional chiral fermi- ons, or non-symmorphic nodal planes, some of which also exhibit chiral charges[19,23,24,27] (Supplementary Sections E and F). Kramers– Weyl fermions enable unusual phenomena, such as a monopole-like electron spin texture and topologically non-trivial bulk Fermi sur- faces over an unusually large energy window. Given the abundance of previously synthesized chiral crystals, our findings are widely applicable and provide another approach to engineering and con- trolling the unconventional optical[7] and transport[5,6] properties in chiral materials.

References

1. Wigner, E. P. On unitary representations of the inhomogeneous Lorentz group. *Ann. Math.* **40**, 149–204 (1939).
2. Bradley, C. J. & Cracknell, A. P. *The Mathematical Theory of Symmetry in Solids* (Clarendon Press Oxford, Oxford, 1972).
3. Flack, H. D. Chiral and achiral crystal structure. *Helv. Chim. Acta* **86**, 905–921 (2003).
4. Bogdanov, A. & Hubert, A. Thermodynamically stable magnetic vortex states in magnetic crystals. *J. Magn. Mater.* **138**, 255–269 (1994).
5. Rikken, G. L. J. A., Fölling, J. & Wyder, P. Electrical magnetochiral anisotropy. *Phys. Rev. Lett.* **87**, 236602 (2001).
6. Yoda, T., Yokoyama, T. & Murakami, S. Current-induced orbital and spin magnetizations in crystals with helical structure. *Sci. Rep.* **5**, 12024 (2015).
7. Fasman, G. D. *Circular Dichroism and the Conformational Analysis of Biomolecules* (Springer, Berlin, 2013).
8. Hasan, M. Z., Xu, S.-Y. & Bian, G. Topological insulators, topological superconductors and Weyl fermion semimetals. *Phys. Scr.* **T164**, 014001 (2015).
9. Zheng, H. & Hasan, M. Z. Quasiparticle interference on type-I and type-II Weyl semimetal surfaces: a review. *Adv. Phys. X* **3**, 146661 (2018).
10. Yang, B. J. & Nagaosa, N. Classification of stable three-dimensional Dirac semimetals with nontrivial topology. *Nat. Commun.* **5**, 4898 (2015).
11. Murakami, S. Phase transition between the quantum spin Hall and insulator phases in 3D: emergence of a topological gapless phase. *New J. Phys.* **9**, 356 (2007).
12. Wan, X. et al. Topological semimetal and Fermi-arc surface states in the electronic structure of pyrochlore iridates. *Phys. Rev. B* **83**, 205101 (2011).
13. Burkov, A. A. & Balents, L. Weyl semimetal in a topological insulator multilayer. *Phys. Rev. Lett.* **107**, 127205 (2011).
14. Young, S. M. et al. Dirac semimetal in three dimensions. *Phys. Rev. Lett.* **108**, 140405 (2012).
15. Mañes, J. L. Existence of bulk chiral fermions and crystal symmetry. *Phys. Rev. B* **85**, 155118 (2012).
16. Fang, C. et al. Multi-Weyl topological semimetals stabilized by point group symmetry. *Phys. Rev. Lett.* **107**, 127205 (2011).
17. Kim, W., Wieder, B. J., Kane, C. L. & Rappe, A. M. Dirac line nodes in inversion-symmetric crystals. *Phys. Rev. Lett.* **115**, 036806 (2015).
18. Watanabe, H. et al. Filling constraints for spin-orbit coupled insulators in symmorphic and nonsymmorphic crystals. *Proc. Natl Acad. Sci. USA* **112**, 14551–14556 (2015).
19. Bradlyn, B. et al. Beyond Dirac and Weyl fermions: unconventional quasiparticles in conventional crystal. *Science* **353**, aaf5037 (2016).
20. Wieder, B. J. et al. Double Dirac semimetals in three dimensions. *Phys. Rev. Lett.* **116**, 186402 (2016).
21. Po, H. C., Vishwanath, A. & Watanabe, H. Topological materials discovery using electron filling constraints. *Nat. Phys.* **14**, 55–61 (2018).
22. Bradlyn, B. et al. Topological quantum chemistry. *Nature* **547**, 298–305 (2017).
23. Chang, G. et al. Unconventional chiral fermions and large topological Fermi arcs in RhSi. *Phys. Rev. Lett.* **119**, 206401 (2017).
24. Tang, P., Zhou, Q. & Zhang, S.-C. Multiple types of topological fermions in transition metal silicides. *Phys. Rev. Lett.* **119**, 206402 (2017).
25. Witczak-Krempa, W., Knap, M. & Abanin, D. Interacting Weyl semimetals: characterization via the topological Hamiltonian and its breakdown. *Phys. Rev. Lett.* **113**, 136402 (2014).

26. Bernevig, B. A. *Lecture on Weyl semimetals at the Topological Matter School, Donostia International Physics Center* (Topological Matter School, 2016); https://tms16.sciencesconf.org/; https://www.youtube.com/watch?v= j0zgWHLL1z4
27. Xiao, M. & Fan, S. Topologically charged nodal surface. Preprint at https://arxiv.org/abs/1709.02363 (2017).
28. Sharma, G. et al. Electronic structure, photovoltage, and photocatalytic hydrogen evolution with p-$CuBi_2O_4$ nanocrystals. *J. Mater. Chem. A* **4**, 2936–2942 (2016).
29. Di Sante, D. et al. Realizing double Dirac particles in the presence of electronic interactions. *Phys. Rev. B.* **96**, 121106(R) (2017).
30. Inorganic Crystal Structure Database (FIZ Karlsruhe, 2014); http://icsd.fiz-karlsruhe.de/icsd
31. Xu, S.-Y. et al. Discovery of a Weyl fermion semimetal and topological Fermi arcs. *Science* **349**, 613–617 (2015).
32. Lv, B. Q. et al. Experimental discovery of Weyl semimetal TaAs. *Phys. Rev. X* **5**, 031013 (2015).
33. Lu, L. et al. Experimental observation of Weyl points. *Science* **349**, 622–624 (2015).
34. Kourtis, S. Bulk spectroscopic measurement of the topological charge of Weyl nodes with resonant x-rays. *Phys. Rev. B* **94**, 125132 (2016).
35. Itoh, S. Weyl Fermions and spin dynamics of metallic ferromagnet $SrRuO_3$. *Nat. Commun.* **7**, 11788 (2016).
36. de Juan, F. et al. Quantized circular photogalvanic effect in Weyl semimetals. *Nat. Commun.* **8**, 15995 (2017).
37. Xiong, J. et al. Evidence for the chiral anomaly in the Dirac semimetal Na_3Bi. *Science* **350**, 413–416 (2014).
38. Soluyanov, A. A. et al. Type-II Weyl semimetals. *Nature* **527**, 495–498 (2015).
39. Chan, C.-K. & Lee, P. A. Emergence of bulk gap and metallic side walls in the zeroth Landau level in Dirac and Weyl semimetals. *Phys. Rev. B* **96**, 195143 (2017).
40. Hu, J. et al. π Berry phase and Zeeman splitting of TaP probed by high field magnetotransport measurements. *Sci. Rep.* **6**, 18674 (2016).
41. Wang, Z. & Zhang, S.-C. Chiral anomaly, charge density waves, and axion strings from Weyl semimetals. *Phys. Rev. B* **87**, 161107(R) (2013).
42. Sun, Y., Zhang, Y., Felser, C. & Yan, B. Giant intrinsic spin Hall effect in the TaAs family of Weyl semimetals. *Phys. Rev. Lett.* **117**, 146403 (2016).
43. Shan, J. & Heinz, T. F. *Ultrafast Dynamical Processes in Semiconductors* (Springer, Berlin, 2004).
44. Zyuzin, A. A. et al. Weyl semimetal with broken time reversal and inversion symmetries. *Phys. Rev. B* **85**, 165110 (2012).
45. Zhong, S., Moore, J. E. & Souza, I. Gyrotropic magnetic effect and the magnetic moment on the Fermi surface. *Phys. Rev. Lett.* **116**, 077201 (2016).
46. Bardarson, J. H., Lu, Y.-M. & Moore, J. E. Superconductivity of doped Weyl semimetals: finite-momentum pairing and electronic analogues of the ^{3}He-A phase. *Phys. Rev. B* **86**, 214514 (2012).
47. Hosur, P. & Qi, X.-L. Time-reversal invariant topological superconductivity in doped Weyl semimetals. *Phys. Rev. B* **90**, 045130 (2014).
48. Xu, S.-Y. et al. Momentum-space imaging of Cooper pairing in a half-Dirac- gas topological superconductor. *Nat. Phys.* **10**, 943–950 (2014).

acknowledgements

Work at Princeton was supported by the US Department of Energy under Basic Energy Sciences (grant no. DOE/BES DE-FG-02-05ER46200). M.Z.H. acknowledges Visiting Scientist support from the Lawrence Berkeley National Laboratory, and partial support for theoretical work from the Gordon and Betty Moore Foundation (grant no. GBMF4547/Hasan). The work at the National University of Singapore was supported by the National Research Foundation, Prime Minister's Office, Singapore, under its NRF fellowship (NRF award no. NRF-NRFF2013-03). B.J.W. acknowledges support through a Simons Investigator grant from the Simons Foundation to C. L. Kane, through Nordita under ERC DM 321031, through grants from the Department of Energy (no. DE-SC0016239), the Simons Foundation (Simons Investigator grant no. ONR- N00014-14-1-0330), the Packard Foundation and the Schmidt Fund to B. A. Bernevig, and acknowledges the hospitality of the Donostia International Physics Center. F.S. and T.N. acknowledge support by the Swiss National Science Foundation (grant no. 200021–169061) and the ERC-StG-Neupert-757867-PARATOP, respectively. T.-R.C. was supported by the Ministry of Science and Technology under the MOST Young Scholar Fellowship: MOST Grant for the Columbus Program no. 107-2636-M-006-004-, National Cheng Kung University, Taiwan, and the National Center for Theoretical Sciences (NCTS), Taiwan. M.Z.H. acknowledges support from the Miller Institute of Basic Research in Science at the University of California at Berkeley in the form of a Visiting Miller Professorship during the early stages of this work. The authors thank C. L. Kane and R. Kamien for helpful discussions on chirality and thank B. Bradlyn, J. Cano, M. I. Aroyo and B. A. Bernevig for insightful discussions on group theory and symmetry.

author contributions

All the authors contributed to the intellectual content of this work. By systematically studying the electronic structures of chiral crystals, the existence of Weyl points at TRIM

points of chiral crystals was recognized by G.C. and S.-Y.X. in consultation with M.Z.H. B.J.W. proved that Weyl fermions at TRIM points (Kramers-Weyl fermions) are a generic feature of all chiral crystals, and thus that all point degeneracies in chiral crystals are topological. F.S. and T.N. proved the relationship between bulk symmetry eigenvalues and the chiral charge of Kramers–Weyl fermions. Spin–momentum locking was proposed by F.S. and T.N., and applied to models and materials by B.J.W., S.-Y.X and G.C. The materials search was done by G.C. and S.-Y.X. with help from all the authors. Tight- binding models were constructed by B.J.W., F.S. and T.N. The first-principles calculations were performed by G.C., S.-M.H., B.S., D.W.,T.-R.C. and H.L. The manuscript was written by G.C., B.J.W., F.S., T.N., S.-Y.X., H.L. and M.Z.H. with the help of D.S.S. and
I.B. S.-Y.X., H.L. and M.Z.H. were responsible for the overall research direction, planning and integration among different research units.

Method
s

We performed first-principles calculations within the density functional theory framework using the projector augmented wave method as implemented in the VASP[49] package and the full-potential augmented plane-wave method as implemented in the package Wien2k[50]. The generalized gradient approximation was used[51]. The lattice constants for the materials examined in this paper were obtained from the ICSD[36]. To calculate the surface states of $AgBi(Cr_2O_7)_2$, Wannier functions were generated using the *d* orbitals of Ag, the *p* and *d* orbitals of Cr and the *p* orbitals of O. The surface states were calculated for a semi-infinite slab by the iterative Green's function method.

To calculate the circular photogalvanic current in α-$Ag_2Se_{0.3}Te_{0.7}$ (SG 19), we generated the Wannier functions of α-Ag_2Se (SG 19) and α-Ag_2Te (SG 19) using the *s* and *d* orbitals of Ag and the *p* orbitals of Se and Te. The electronic structure of α-$Ag_2Se_{0.3}Te_{0.7}$ (SG 19) was calculated by a linear interpolation between tight- binding model matrix elements of α-Ag_2Se (SG 19) and α-Ag_2Te (SG 19). We calculated the multiband gyrotropic photocurrent tensor $\beta_{ij}(\omega)$ (ref. [36]) to obtain the circular photogalvanic effect photocurrent rate:

$$\beta_{ij}(\omega) = \frac{i e^3}{\hbar} \sum_{jkl} \sum_{nm} \int_{\mathbf{k},n,m} f_{\mathbf{k}} i \, r^{\mathbf{k}}_{\mathbf{k},nm} r^{l}_{k,nm} (-E_{\mathbf{k},mn}) \quad (5)$$

Data availability

The data supporting the findings of this study are available within the paper and other findings of this study are available from the corresponding author upon reasonable request.

References

49. Kresse, G. & Furthmöller, J. Efficiency of ab-initio total energy calculations for metals and semiconductors using a plane-wave basis set. *Comput. Mater. Sci.* **6**, 15–50 (1996).
50. Blaha, P., Schwarz, K. & Madsen, G. K. H. et al. *An Augmented Plane Wave plus Local Orbital Program for Calculating Crystal Properties*. (Vienna University of Technology, Vienna, 2001).
51. Perdew, J. P., Burke, K. & Ernzerhof, M. Generalized gradient approximation made simple. *Phys. Rev. Lett.* **77**, 3865 (1996).